Supplementary Information

Photoswitchable stable charge-distributed states in a new Cobalt complex exhibiting photo-induced valence tautomerism

Michael Slota,[a,b*] Marian Blankenhorn,[a] Eric Heintze,[a] Minh Vu,[a] Ralph Hübner,[a] and Lapo Bogani[b*]

Received Xth XXXXXXXXXX 20XX, Accepted Xth XXXXXXXXX 20XX
First published on the web Xth XXXXXXXXXX 20XX
DOI: 10.1039/c000000x

1 Results from DFT calculations

Full geometry optimizations of the complexes were carried out using the density functional theory method (DFT) at the B3LYP level[1]. All atoms were assigned a 6-31G* basis set and calculations were performed with Spartan'14 program packages[2].

The calculations show an increase of the bond lengths between the cobalt and the oxygen atoms of 0.19 Å at the LS to HS transition, while the ones between the oxygen and the carbon atoms decrease for 0.05 Å.

[a] *1. Physikalisches Institut, University of Stuttgart, Pfaffenwaldring 57, 70569 Stuttgart, Germany. Tel: +49(0)711-68564891; E-mail: michael.slota@pi1.physik.uni-stuttgart.de*
[b] *Department of Materials, University of Oxford, 16 Parks Road, OX1 3PH, Oxford, United Kingdom. Tel: +44(0)1865-283341; E-mail: lapo.bogani@materials.ox.ac.uk*

Table 1 Bond lengths of **1** in LS and HS configuration.

	LS-Co(III) [Å]	HS-Co(II) [Å]
Co – N(1)	1.968	2.140
Co – N(2)	1.961	2.145
Co – O(1)	1.873	2.060
Co – O(2)	1.856	2.049
Co – O(10)	1.864	2.059
Co – O(20)	1.877	2.050
O(1) – C(1)	1.324	1.290
O(2) – C(6)	1.317	1.288
C(1) – C(2)	1.423	1.438
C(2) – C(3)	1.391	1.385
C(3) – C(4)	1.424	1.431
C(4) – C(5)	1.387	1.383
C(5) – C(6)	1.408	1.415
C(1) – C(6)	1.438	1.472
O(10) – C(11)	1.339	1.290
O(20) – C(16)	1.331	1.288
C(11) – C(12)	1.415	1.440
C(12) – C(13)	1.401	1.381
C(13) – C(14)	1.412	1.435
C(14) – C(15)	1.397	1.379
C(15) – C(16)	1.398	1.420
C(11) – C(16)	1.430	1.470

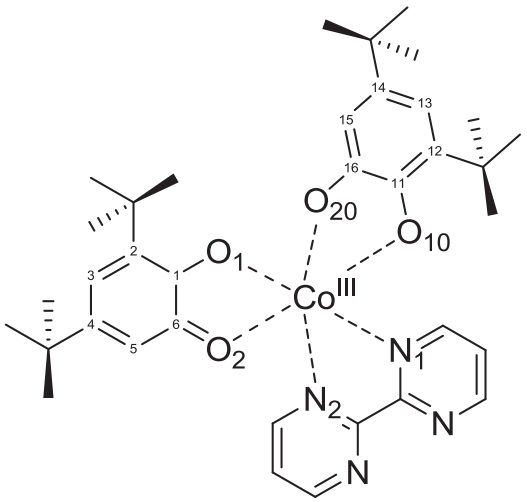

2 Magnetic characterization of different sample preparations

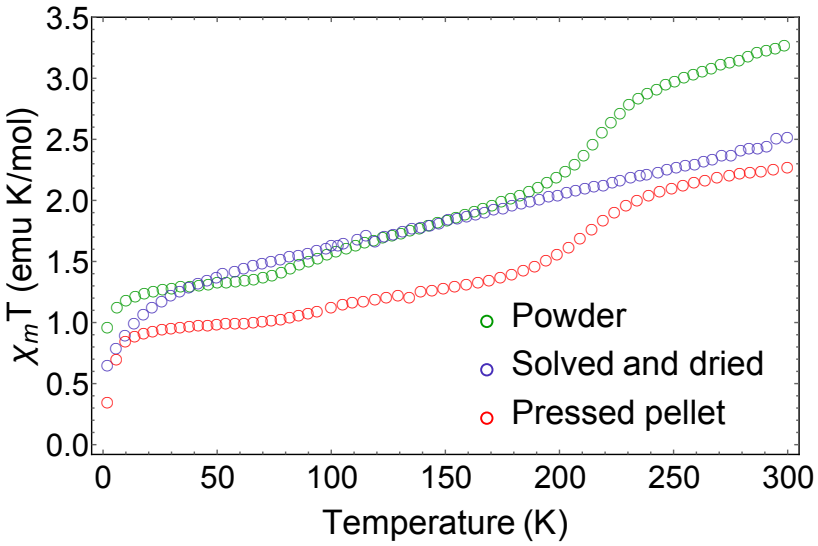

Fig. SI1 SQUID measurement of $\chi_m T$ of **1** in powder form, solved in dichloroethane and dried on a thin glass platelet and as a pressed pellet. The solved complex lost its VT properties as no transition can be observed. The powder shows an increased susceptibility, which is caused by rearrangements in an external field. The VT property in the pellet form is partially quenched as the magnetization changes are smaller compared with the powder sample (see also Fig. 5).

3 EPR signals at various temperatures

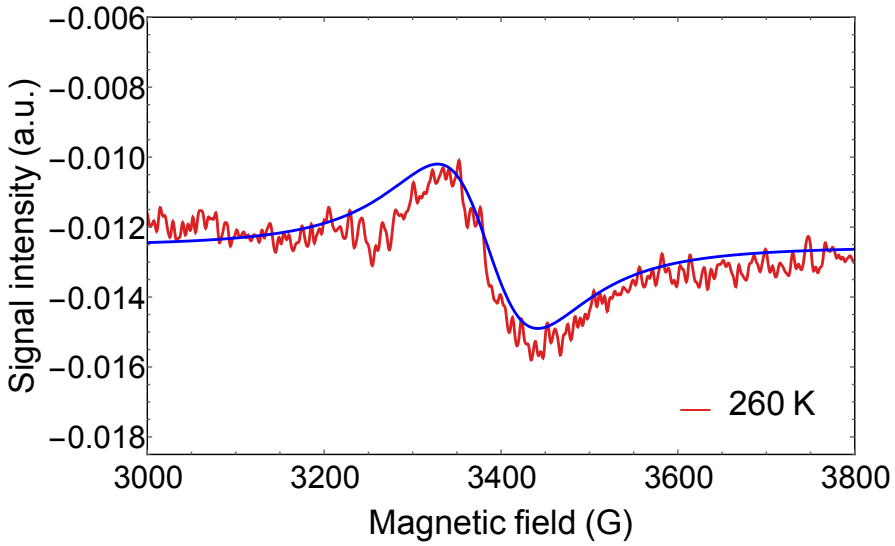

Fig. SI2 EPR signal strength of **1** at 260 K. At higher temperatures, the EPR signal is not detectable. Resonance field: $B_{res} = 3384.9$ G.

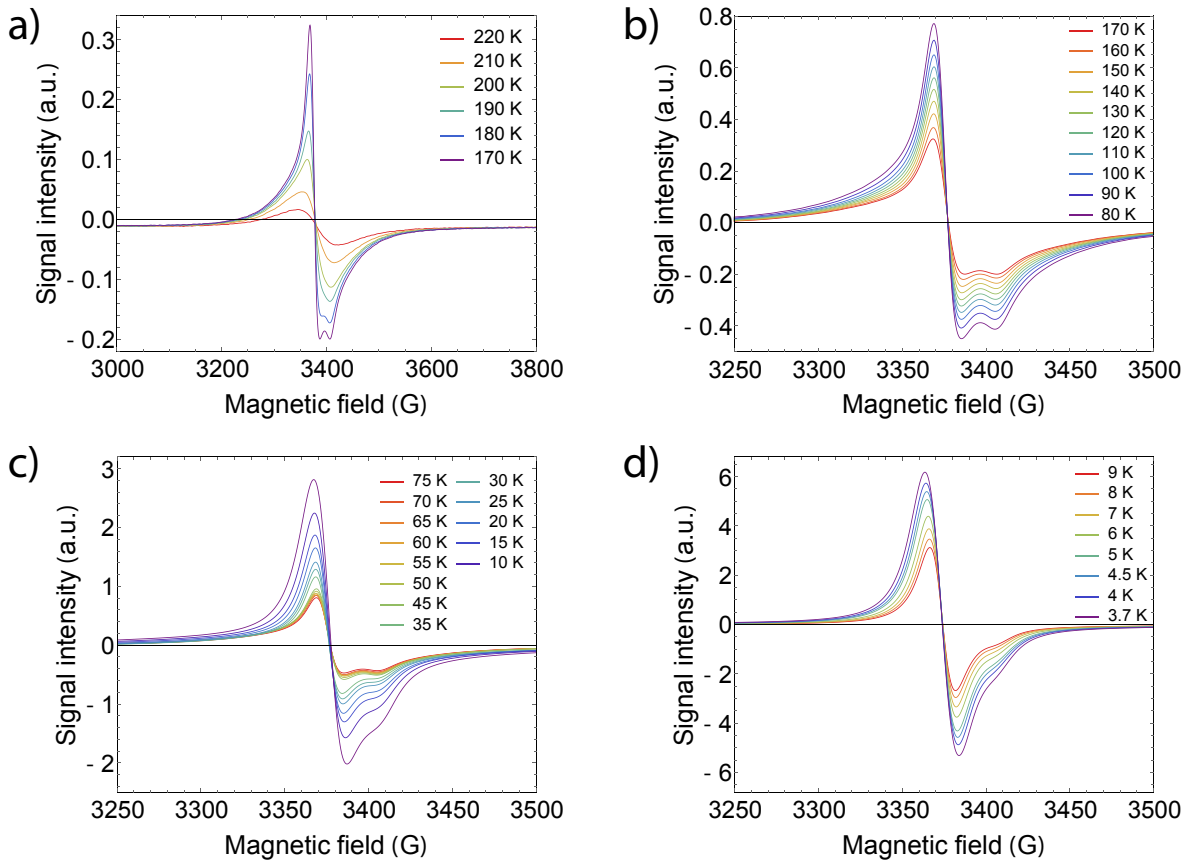

Fig. SI3 EPR signal strength of **1** at different temperatures. Below 220 K, the Lorentzian shaped derivative signal becomes asymmetric, as the signal is superimposed by two Lorentzians explicitly visible below 180 K. Below 10 K a recalibration of the system has been performed, after which the signal intensities of the two transitions slightly changed.

4 EPR spectrum below 3000 G

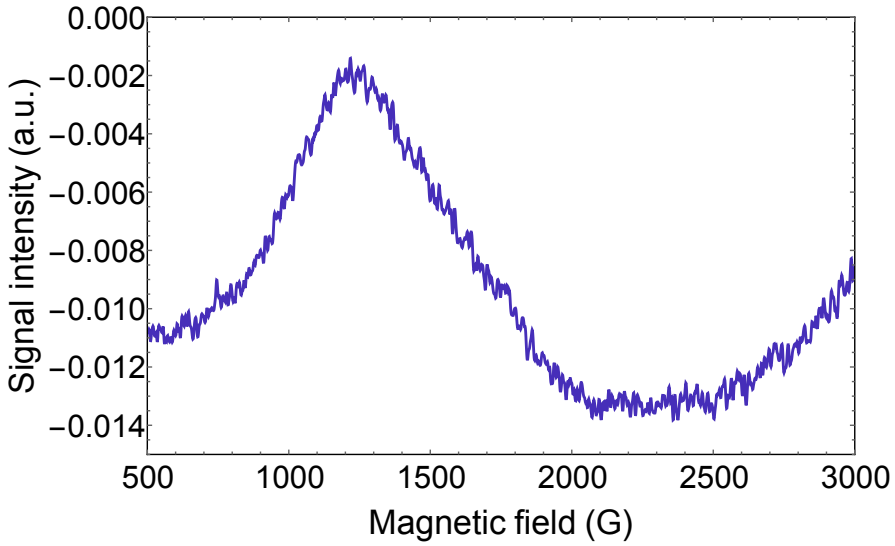

Fig. SI4 The EPR spectrum recorded at 3.75 K and 30 dB attenuation shows an additional weak signal below 3000 G centered around 1700 G. The signal could correspond to a transition with $g = 4$ and accordingly $\Delta M = \pm 2$ arising from exchange coupling of the radical ligands[3]. The asymmetry is due to the about 500 times stronger signal at 3376 G at the same conditions.

5 SQUID magnetometry at different laser powers

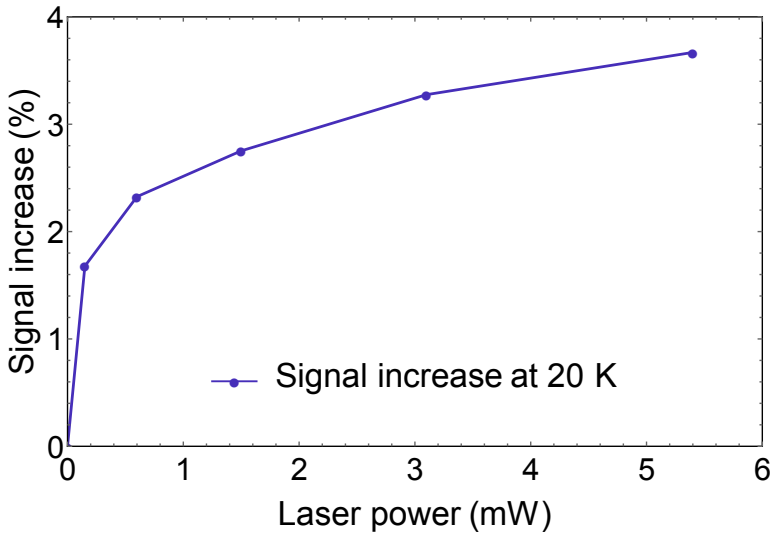

Fig. SI5 Light power dependence of the magnetization change at 20 K after illuminating a pellet sample of **1** for 90 min on the SQUID magnetometer. The power dependence shows that the conversion efficiency increases only slowly for powers above 2 mW. As laser powers beyond 5 mW comes along with strong heating effects, a better way to increase efficiency is to optimize the preparation of the sample.

6 Time evolution of the EPR signal under irradiation

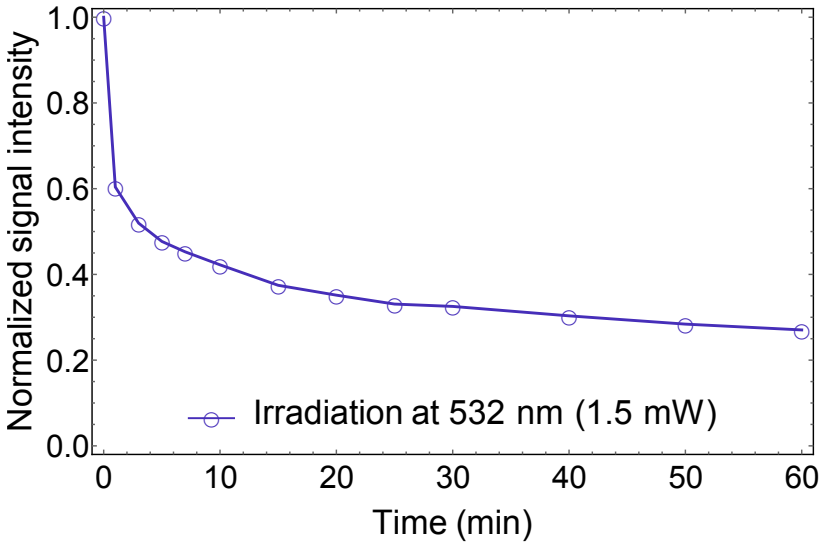

Fig. SI6 Signal change of the EPR line while irradiation at 3.5 K. The signal strength decreases with irradiation time as the generated LS to HS transition produces EPR-silent $(SQ)_2$ species.

7 UV/Vis/NIR diagram

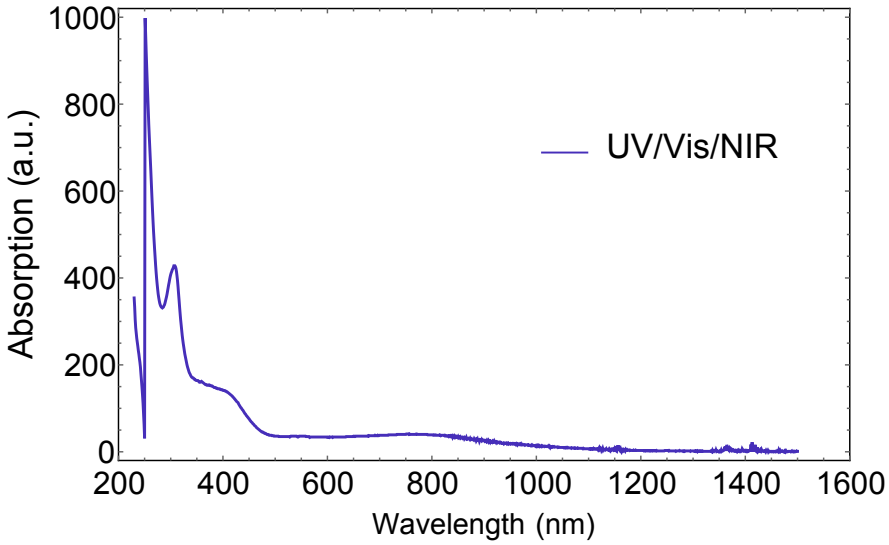

Fig. SI7 UV/Vis/NIR absorption of **1**. The measurement has been carried out on an UV 160 (Shimadzu) spectrometer at room temperature at a range from 200 nm to 1500 nm. The sample was prepared in a HELMA cuvette made of quartz glass with a thickness of 10 mm.

8 Signal strength upon attenuation

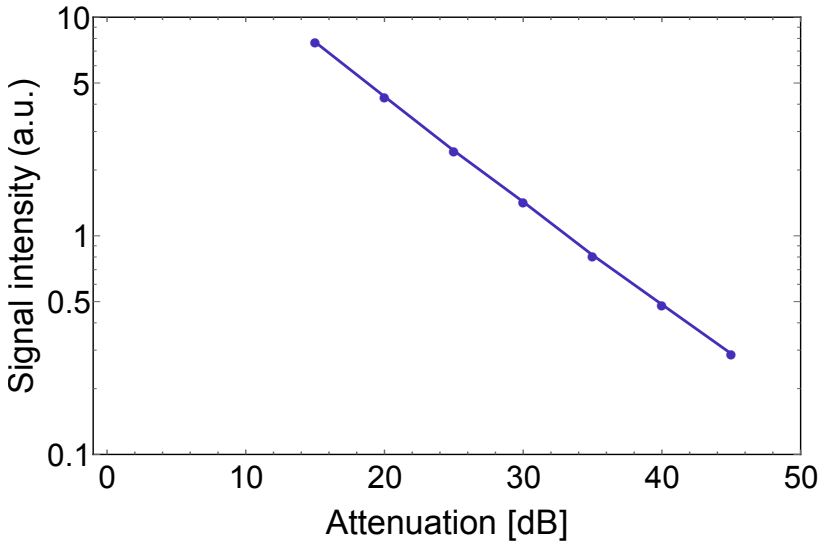

Fig. SI8 The EPR signal strength decreases linearly with attenuation and a constant receiver gain of 30 at the attenuations used throughout this work. The linear behavior proves that all measurements were performed in a non-saturating regime.

9 Exemplary fit of EPR data

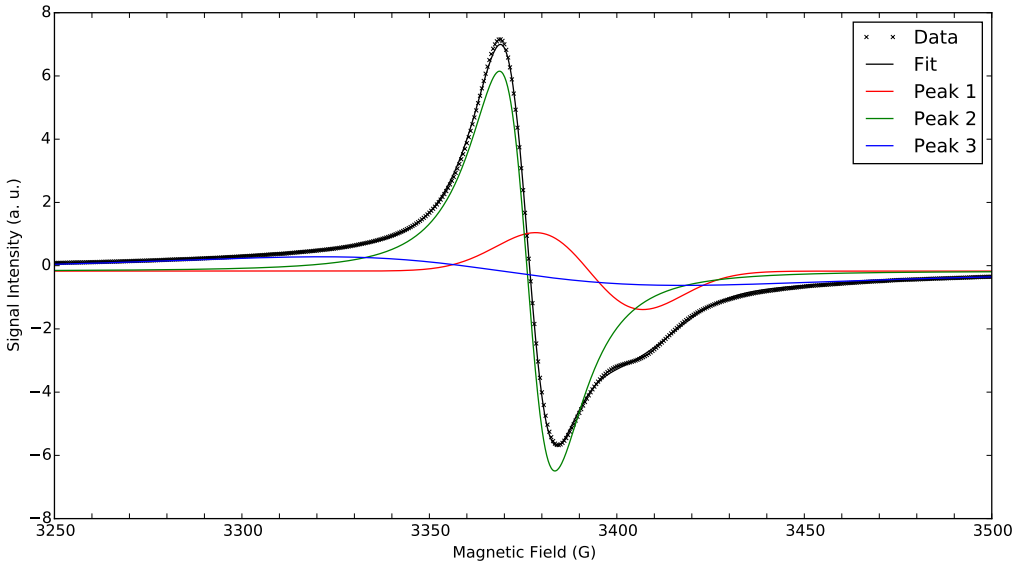

Fig. SI9 Fit of the EPR signal strength at 20 K. Three Lorentzians were necessary to fit the data, where mainly curve 1 and 2 account for investigated transitions in this work.

10 Field dependence of magnetic moment

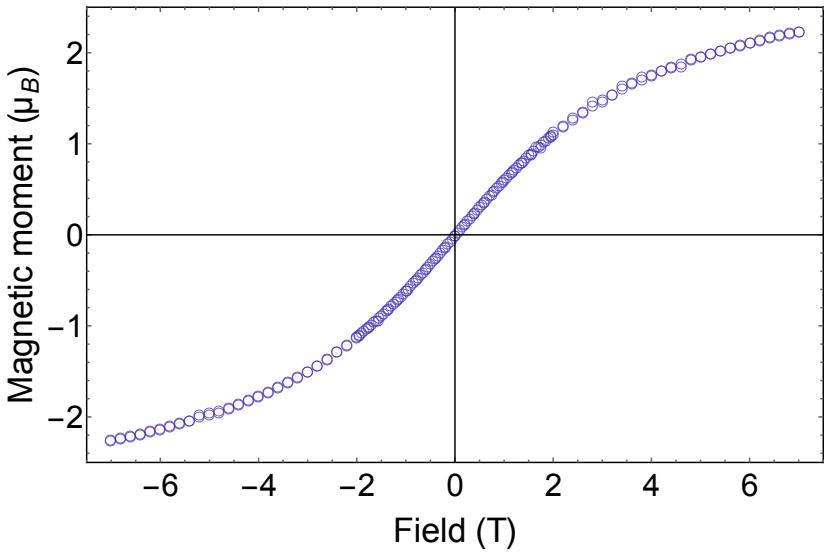

Fig. SI10 The field dependence of the magnetic moment recorded at 5 K does not show any hysteresis behavior.

11 Change of magnetic moment with time

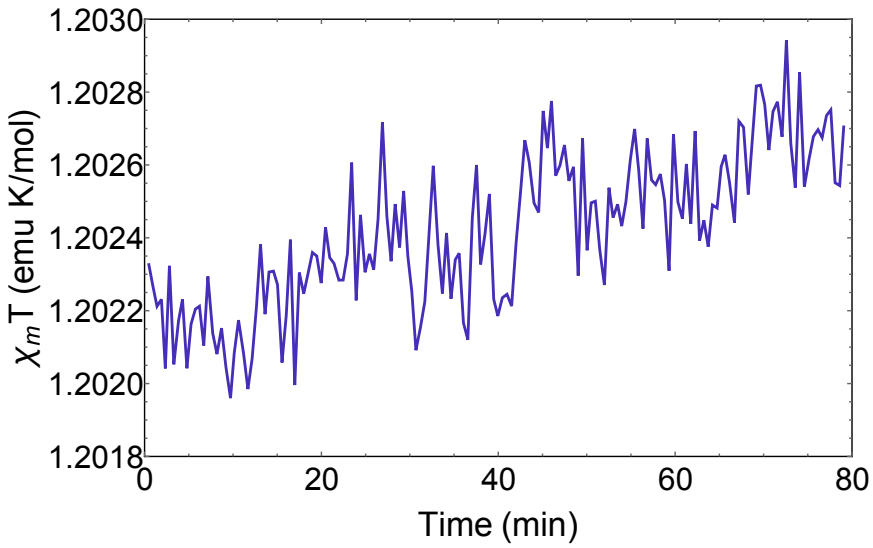

Fig. SI11 The $\chi_m T$ value, recorded at 15 K, increases with time at a constant magnetic field (here 5000 Oe). The increase can be resetted when warming up to 300 K and turning off the magnetic field for many hours.

References

1 W. Kohn, A. D. Becke and R. G. Parr, *J. Phys. Chem.*, 1996, **100**, 12974–12980.
2 Y. Shao *et al.*, *Phys. Chem. Chem. Phys.*, 2006, **8**, 3172–3191.
3 M. Affronte, A. Beni, A. Dei and L. Sorace, *Dalton Trans.*, 2007, **45**, 5253–5259.